A Theory for the Limitation of ENSO Predictability Due to Stochastic Atmospheric Transients

RICHARD KLEEMAN

Bureau of Meteorology Research Centre, Melbourne, Victoria, Australia

ANDREW M. MOORE

Nova Southeastern University Oceanographic Center, Dania, Florida

(Manuscript received 28 December 1995, in final form 10 July 1996)

ABSTRACT

It is argued that a major fundamental limitation on the predictability of the El Niño–Southern Oscillation phenomenon is provided by the stochastic forcing of the tropical coupled ocean–atmosphere system by atmospheric transients. A new theoretical framework is used to analyze in detail the sensitivity of a skillful coupled forecast model to this stochastic forcing. The central concept in this analysis is the so-called stochastic optimal, which represents the spatial pattern of noise most efficient at causing variance growth within a dynamical system. A number of interesting conclusions are reached. (a) Sensitivity to forcing is greatest during the northern spring season and prior to warm events. (b) There is little sensitivity to meridional windstress noise. (c) A *western* Pacific dipole pattern in heat flux noise is most efficient in forcing *eastern* Pacific SST variance. An estimate of the actual wind stress stochastic forcing is obtained from recent ECMWF analyses and it is found that ''unavoidable'' error growth within the model due to this stochastic forcing saturates at approximately 0.5°C in the NINO3 region with very rapid error growth during the first 6 months. The noise projects predominantly onto the first stochastic optimal and, in addition, around 95% of the error growth can be attributed to stochastic forcing with a strong synoptic character.

1. Introduction

The study of the nature of atmospheric flow predictability is now quite a developed field. The work of Lorenz about 30 years ago established that weather forecasts beyond a certain duration are extremely sensitive to the specification of initial conditions and that this sensitivity provides a fundamental limitation to the predictability of the flow. A large amount of effort has been devoted in the literature to understanding this rapid error growth. One particular school (e.g., Frederiksen 1982) has focused on the study of the so-called normal modes of the dynamical system, which consist of the eigenvectors of the linearized matrix **A** that satisfy the equation

$$\frac{\partial \mathbf{u}}{\partial t} = \mathbf{A}\mathbf{u},$$

where **u** is the linearization vector of the dynamical system under consideration. The most unstable of such modes tends to dominate error growth given sufficient time. On the other hand, others, such as Farrell (1990) and Molteni and Palmer (1993), have emphasized the ''singular vectors'' or ''optimals'' of the system. These are the eigenvectors of the self-adjoint operator $B^*(T)B(T)$, where $B(T)$, the propagator operator, translates the dynamical state vector **u** forward T time units.[1] The singular vectors with the greatest eigenvalues give the spatial patterns of initial condition errors that grow by the greatest amount over the specified time period. Interestingly, there exist realistic systems that possess no unstable normal modes but still possess growing singular vectors for values of T of interest to forecasting.

Another perspective has been provided by Egger and Schilling (1984), who have been interested in studying the predictability of the low-frequency planetary-scale part of the flow. In their framework, they consider the high-frequency synoptic-scale atmospheric motion as providing a stochastic forcing to the planetary-scale modes and hence acting as a fundamental limit to their predictability.

In this paper we shall argue that this stochastic per-

Corresponding author address: Dr. Richard Kleeman, Bureau of Meteorology Research Centre, GPO Box 1289K, Melbourne, Victoria 3001, Australia.
E-mail: rzk@bom.gov.au

[1] The operators A and B are related in the limit so that T becomes very small by the relation $B(\Delta t) = 1 + \Delta t A$.

spective on error growth is an appropriate one for the El Niño–Southern Oscillation (ENSO) phenomenon. In the paradigm to be advocated, the role of stochastic forcing is provided by atmospheric transients. This forcing projects onto the very low frequency coupled ocean–atmosphere modes, which consequently limits multiseasonal predictability.

The study of predictability in the ENSO context is still very much in its infancy. This state of affairs is hardly surprising given that dynamical models capable of forecasting the phenomenon have only existed now for a decade. The first model shown to have this capability was the intermediate model of Zebiak and Cane (1987). Interestingly, such models (see also Kleeman et al. 1995) are still able to out-perform quite sophisticated general circulation models despite having some quite large simplifications in their model physics. Such a situation probably indicates that a relatively simple physical mechanism is responsible for a good deal of ENSO variability (see Kleeman 1993).

Given the success of intermediate models and also their relative inexpense, most studies of ENSO error growth/predictability have been based around them. The works of Goswami and Shukla (1991) and Blumenthal (1991), for example, were concerned with initial condition error growth within such models.

While these models may have the dominant process responsible for reasonably *simulating* ENSO, it is not clear they contain the mechanisms responsible for *limiting* its predictability. A particular concern in this regard has been the absence of model atmospheric transients. Intermediate models [and also many hybrid models such as Balmaseda et al. (1994)] have steady-state atmospheric models, which essentially give a unique solution for atmospheric flow when forced with a given SST pattern. This is in contrast to atmospheric general circulation models and the real atmosphere, where a large ensemble of different flows are possible. In general, the *mean* of this ensemble is close to the flow predicted by the steady-state simple atmospheric models, which allows such models to work reasonably well (e.g., Kleeman 1991; Kleeman et al. 1992). Note also that the particular member of the ensemble that will occur in several months' time is essentially unpredictable given the known limits to predictability of atmospheric flows discussed previously. Thus inclusion of a realistic simulation of the ensemble will not necessarily assist in multiseasonal prediction.[2] On the other hand, it seems reasonable to expect that omitting internal atmospheric variability within a coupled model will lead to a possibly serious underestimate of error growth within the real coupled system.

As a first step towards examining this issue, Kleeman and Power (1994) obtained an estimate of the windstress noise and added it to the windstress derived from the Kleeman (1993) intermediate coupled model. They showed that the resultant error growth within the model occurred at fairly rapid rate (on the order of months) and tended to saturate at a significant level after the initial growth. Such a response is typical of a stochastically driven system. The degree of error growth obtained from this stochastic mechanism can be shown to be far greater than that obtained when the initial conditions of the model alone are subject to small random errors. Displayed in Fig. 1 is the error growth resulting from perturbing the initial conditions of a large ensemble of coupled model forecasts by random zonal and meridional wind ''errors'' of standard deviation 0.2 m s^{-1}. The initial conditions were prepared by spinning up the ocean model with historical wind data and had dates 3 months apart for the entire period of 1972–86. The figure shows how errors in the NINO3 (150°W to 90°W and 5°N to 5°S) SST anomaly index region evolve

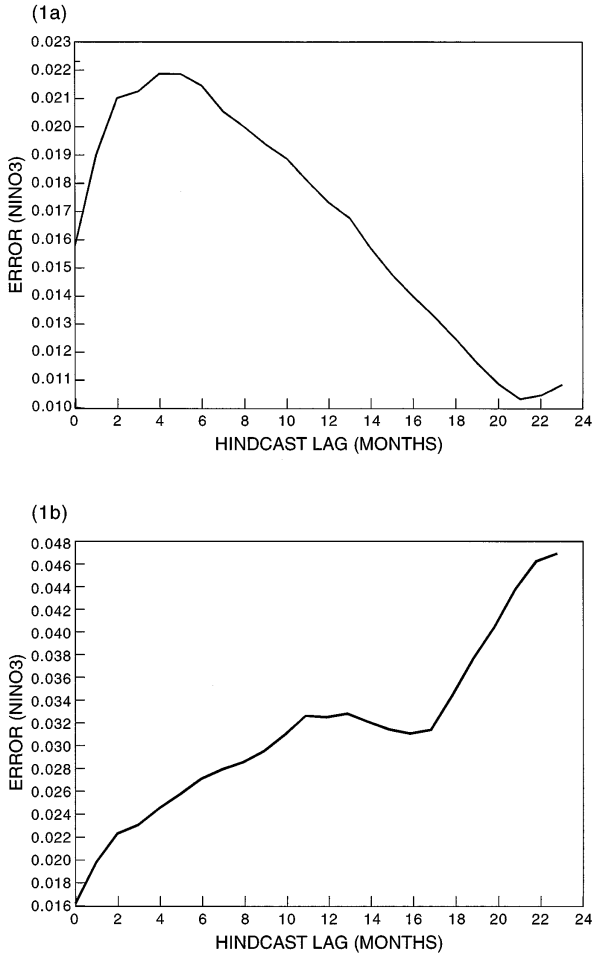

FIG. 1. (a) The ensemble rms error growth of the standard coupled model after perturbation of initial conditions (see text). (b) Identical to (a) but with increased coupling strength (see text). Errors refer to NINO3 values and are in °C.

[2] Unless, of course, the inclusion of the ensemble improves the mean response.

when the coupling strength of the model is at its standard value and when the coupling strength is increased by around 50%. Two values were chosen because they are on either side of the self-sustaining oscillation bifurcation of the model. The results indicate only very modest error growth whether the model has self-sustaining oscillations or not. These figures are to be compared with those from Fig. 8 of Kleeman and Power (1994), which show the same ensemble experiments but with an estimate of wind stress noise causing ensemble divergence. There is much greater error growth in the latter case with errors approaching 0.5°C after around 4 months. It is interesting to note that in a nearly identical initial condition experiment to that described above, Goswami and Shukla (1991) found greater error growth in the Zebiak and Cane (1987) coupled model with errors increasing more or less linearly to around 0.5°C at 24 months. Note that such growth is still considerably less rapid than that reported by Kleeman and Power (1994). The most likely explanation for this difference in behavior of the two models lies in the apparently chaotic-like behavior of the Zebiak and Cane model (see Zebiak and Cane 1991) that is in contrast to the Kleeman model, which exhibits only regular oscillations. In this respect, the Kleeman model is more similar to the Battisti (1988) intermediate model. The issue of chaotic behavior by coupled models has been addressed in some detail by Jin et al. (1994) and F.-F. Jin et al. (1996, personal communication), who used an intermediate coupled model similar to the Kleeman model. In the latter paper, they conducted a rather large survey of parameter space in order to locate chaotic regimes. While they found a number of such regimes, they concluded that these tended to occupy a rather small part of parameter space. This was in contrast to regular oscillatory behavior, which tended to dominate most of the space surveyed. Such a result suggests that the real coupled system may be more likely to exhibit the very small initial condition error growth depicted here, although such a conclusion is, of course, preliminary given the simplicity of the models studied.

In related work, Penland and Sardeshmukh (1995) have argued on the basis of historical SST data that the ENSO phenomenon itself can be described as a stable dynamical system driven by spatially coherent Gaussian noise. They argue that the stochastic forcing sets up an optimal initial structure that then grows via the constructive interference of damped normal modes within the system.

In this paper we shall take the previous study of Kleeman and Power (1994) one step further by outlining a theoretical framework that shall allow us to obtain insight into the dynamical mechanisms by which stochastic atmospheric fluxes of both momentum and heat cause error growth within the coupled system. The framework outlined is a small extension of that recently proposed in the atmospheric context by Farrell and Ioannou (1993a). It shall also allow us to relate the stochastic theory to the insights recently obtained by Moore and Kleeman (1996) in their study of the singular vectors of the Bureau of Meteorology Research Centre (BMRC) intermediate coupled model.

The rest of the paper is organized as follows. Section 2 provides a derivation and overview of the theoretical framework to be used. Section 3 describes the so-called stochastic optimals of the coupled model and their sensitivity to the seasonal cycle and ENSO phase. Section 4 discusses the nature of the wind stress noise and its projection onto the optimals, while section 5 contains a summary and discussion of the results obtained.

2. Theoretical framework

We provide here a relatively brief and hopefully intuitive outline of the theoretical results required from stochastic dynamical theory. Other results with a somewhat different emphasis may be found in the recent publications by Farrell and Ioannou (1993a–c).

We shall confine our treatment to time-discretized versions of partial differential equations in order to keep the derivation transparent. The derivations are easily extended to the continuous case (see Kleeman et al. 1988).

We assume that the dynamical system of interest can be modeled by the following linear stochastic differential equation:

$$\mathbf{u}(t) = \mathbf{A}(t)\mathbf{u}(t) + \mathbf{f}(t), \tag{1}$$

where $\mathbf{f}(t)$ is a Gaussian noise with zero mean for all times; we are using boldface to indicate matrices/vectors with respect to spatial and vector indices. Matrices are denoted by upper case symbols while vectors are lower case.

Consider now a backward time discretization of Eq. (1) and label the time indices with Greek letters:

$$\mathbf{u}_{\mu+1} = \mathbf{u}_\mu + \Delta t(\mathbf{A}_\mu\mathbf{u}_\mu + \mathbf{f}_\mu). \tag{2}$$

This may be rewritten as

$$\mathbf{u}_{\mu+1} = \mathbf{B}(\mu + 1, \mu)\mathbf{u}_\mu + \Delta t\mathbf{f}_\mu, \tag{3}$$

where $\mathbf{B}(\nu, u)$ is referred to as the propagator matrix from time μ to ν, as applying it to $\mathbf{u}_\mu$ in the unforced case produces $\mathbf{u}_\nu$. Mathematically, we have $\mathbf{B}(\nu, u) = (1 + \Delta t\mathbf{A}_{\nu-1})(1 + \Delta t\mathbf{A}_{\nu-2}) \cdots (1 + \Delta t\mathbf{A}_\mu)$.

It is relatively straightforward now to write $\mathbf{u}_\mu$ as a function of $\mathbf{f}$. This can be obtained by iterating (3) from a set of initial conditions:

$$\mathbf{u}_\mu = \mathbf{B}(\mu, 0)\mathbf{u}_0 + \Delta t \sum_{\lambda=0}^{\mu-1} \mathbf{B}(\mu, \lambda + 1)\mathbf{f}, \tag{4}$$

where the superscripts are matrix powers. For our present purpose we shall assume that the initial conditions are deterministic, although it should be noted that the subsequent expressions can be generalized to a case where they have prescribed statistics.

If we assume that the noise is specified by the statistics

$$\langle f_{j\lambda} \rangle = 0$$
$$\langle f_{i\mu} f_{j\nu} \rangle = C_{ij}^{\mu\nu} \tag{5}$$

(the angle brackets denote an ensemble average, and we are using Latin indices for the spatial/vector variation), it is easy to derive from (4) an equation for the second order moments

$$\langle \mathbf{u}_\mu \mathbf{u}_\nu^\dagger \rangle = (\Delta t)^2 \sum_{\lambda=0}^{\mu-1} \sum_{\pi=0}^{\nu-1} \mathbf{B}(\mu, \lambda + 1) \mathbf{C}^{\lambda\pi} \mathbf{B}^\dagger(\nu, \pi + 1) + \mathbf{B}(\mu, 0)\mathbf{u}_0(\mathbf{B}(\nu, 0)\mathbf{u}_0)^\dagger. \tag{6}$$

Note that the first moment (the mean) is trivial to evaluate:

$$\langle \mathbf{u}_\mu \rangle = \mathbf{B}(\mu, 0)\mathbf{u}_0, \tag{7}$$

and this implies that the covariance $\langle \mathbf{u}_\mu, \mathbf{u}_\nu^\dagger \rangle = \langle \mathbf{u}_\mu \mathbf{u}_\nu^\dagger \rangle - \langle \mathbf{u}_\mu \rangle \langle \mathbf{u}_\nu^\dagger \rangle$ is simply given by the first term on the right-hand side of Eq. (6). This result generalizes the results of Gardiner (1985) and Farrell and Ioannou (1993a) to the case of nonwhite stochastic forcing. For the purposes of this section we shall assume that the forcing noise is separable in space and time:

$$\mathbf{C}^{\lambda\pi} \equiv \mathbf{C} D^{\lambda\pi}. \tag{8}$$

Using Eq. (6) we can write the covariance at time step μ as

$$\langle \mathbf{u}_\mu, \mathbf{u}_\nu^\dagger \rangle = (\Delta t)^2 \sum_{\lambda=0}^{\mu-1} \sum_{\pi=0}^{\mu-1} D^{\lambda\pi} \mathbf{B}(\mu, \lambda + 1) \cdot \mathbf{C}\mathbf{B}^\dagger(\mu, \pi + 1). \tag{9}$$

It can now be shown easily that the variance at time step μ for a particular norm of interest may be written as

$$\mathrm{Var}(\|\mathbf{u}\|^2) = (\Delta t)^2 \mathrm{Tr}\left\{ \sum_{\lambda=0}^{\mu-1} \sum_{\pi=0}^{\mu-1} D^{\lambda\pi} \mathbf{B}^\dagger(\mu, \lambda + 1) \cdot \mathbf{X}\mathbf{B}(\mu, \pi + 1)\mathbf{C} \right\}, \tag{10}$$

where the matrix $\mathbf{X}$ is the *kernel* of the norm under consideration. If one was interested in the variance of the L_2 norm of the dynamical variables, then $\mathbf{X}$ is the Kronecker delta. On the other hand, if one is interested in the spatial average of a particular dynamical variable such as the SST in the NINO3 region (as we shall be below), then

$$X_{ij} \equiv R_i R_j$$
$$R_i = 1/n \quad \text{if } i \text{ lies in the region of } n \text{ grid points}$$
$$= 0 \quad \text{otherwise.} \tag{11}$$

Equation (10) may be abbreviated in an obvious manner to

$$\mathrm{Var} = \mathrm{Tr}\{\mathbf{ZC}\}$$

with

$$\mathbf{Z} = (\Delta t)^2 \sum_{\lambda=0}^{\mu-1} \sum_{\pi=0}^{\mu-1} D^{\lambda\pi} \mathbf{B}^\dagger(\mu, \lambda + 1) \mathbf{X} \mathbf{B}(\mu, \pi + 1). \tag{12}$$

We have chosen to split the matrix product of 10 into $\mathbf{Z}$ and $\mathbf{C}$ because we wish to clearly separate the influence of the dynamics (expressed through $\mathbf{Z}$) and the stochastic forcing (expressed through $\mathbf{C}$, the spatial covariance matrix) in inducing variance growth in the system.

If $\mathbf{Z}$ and $\mathbf{C}$ have eigenvalue, normalized eigenvector sets $\{q^i, \mathbf{r}^i\}$ and $\{p^i, \mathbf{s}^i\}$, respectively, then

$$tr\{\mathbf{ZC}\} = q^i p^j (\mathbf{r}^i, \mathbf{s}^j)^2, \tag{13}$$

where the round brackets denote the usual vector inner product, and we are summing over repeated Latin indices. This result follows from the result of Hadley (1961, p. 248) that the symmetric matrices $\mathbf{Z}$ and $\mathbf{C}$ may be written as $Z_{ij} = q^k r_i^k r_j^k$ and $C_{ij} = p^k s_i^k s_j^k$. Finally, it is relatively straightforward to establish that the eigenvalues q^k and p^k are all positive (see appendix).

Equations (12) and (13) have a quite simple physical interpretation: the eigenvectors of the noise $\mathbf{s}^i$, which are termed the EOFs, cause a growth in the variance of a variable of interest (e.g., SST in NINO3) by projecting onto the stochastic optimals $\mathbf{r}^i$. This projection is weighted by the variance p^j of the EOF $\mathbf{s}^j$ and by q^i, which measure the degree of instability or excitability of the stochastic optimal $\mathbf{r}^i$. The terminology stochastic optimal is used for the $\mathbf{r}^i$ since noise with the spatial/vector coherence of this eigenvector will be efficient at forcing variance growth within the dynamical system. In particular, noise with the spatial coherency of the stochastic optimal with largest eigenvalue q^i will be most efficient at forcing variance growth within the system. We use a different terminology in this context from that of Farrell and Ioannou (1993a), who refer to stochastic optimals as back EOFs or forcing orthogonal functions (FOFs). The reason for our choice of terminology is the close relationship of stochastic optimals to conventional optimals (see below). Also note that the stochastic optimals introduced here generalize the FOFs of Farrell and Ioannou to the case of any noise that is separable in space and time from the special case of white noise (which, by definition, has zero temporal correlation at any nonzero lag).

The relationship between the two kinds of optimal (stochastic and conventional) is quite apparent when white noise is considered. For such noise we write

$$D^{\lambda\pi} = \frac{1}{\Delta t} \delta^{\lambda\pi},$$

which becomes a delta function as $\Delta t \to 0$, as required for white noise. The stochastic optimal matrix **Z** then reduces to

$$\mathbf{Z} = \Delta t \sum_{\lambda=0}^{\mu-1} \mathbf{B}^{\dagger}(\mu, \lambda + 1)\mathbf{X}\mathbf{B}(\mu, \lambda + 1), \quad (14)$$

which is simply the discretized time integral of the conventional optimal matrices. One might expect therefore that the white noise stochastic optimals at time T are roughly the time average of the conventional optimals for all times between 0 and T. Such an interpretation makes intuitive sense since the system here is being perturbed independently at every time step rather than simply at the first step (or initial conditions), as is the case for conventional error growth studies.

3. Stochastic optimals

In this section we calculate the eigenvectors and eigenvalues of the stochastic optimal matrix Z defined in Eqs. (10) and (12) of the previous section. We shall do this for linearizations of the BMRC intermediate coupled model that is described in detail in Kleeman (1991) and Kleeman (1993) and in summary form in Kleeman and Power (1994).

The model consists of anomaly ocean and atmosphere models that exchange wind and SST and whose dynamics are given by shallow-water equations. The atmospheric model includes a simple convection parameterization that has the effect of causing a realistically nonlinear wind response to SST anomalies. Anomalies in regions of high mean SST, such as the western equatorial Pacific, induce a much larger model response than those in areas of low mean SST, such as the southeastern Pacific.

The ocean model is a tropical Pacific basin model whose dynamics are expressed in terms of equatorial meridional (Kelvin/Rossby) modes and is truncated at the sixth Rossby mode. The prognostic SST equation is influenced only by equatorial thermocline perturbations (which are more important in the east than the west) and a Newtonian cooling term. The meridional structure of SST anomalies is taken to be fixed (symmetric Gaussian with a 10° e-folding radius), and thus anomalies are determined by their equatorial value. A capping nonlinearity is applied to thermocline perturbations in the SST equation to prevent runaway linear coupled instability.

This model with only thermocline perturbations affecting SST was shown in Kleeman (1993) to have optimal skill in forecasting ENSO, and the level of skill obtainable is comparable with the better current international efforts[3] (see Kleeman et al. 1995). It is used routinely within BMRC to produce real time forecasts of the NINO3 index (see Kleeman 1994).

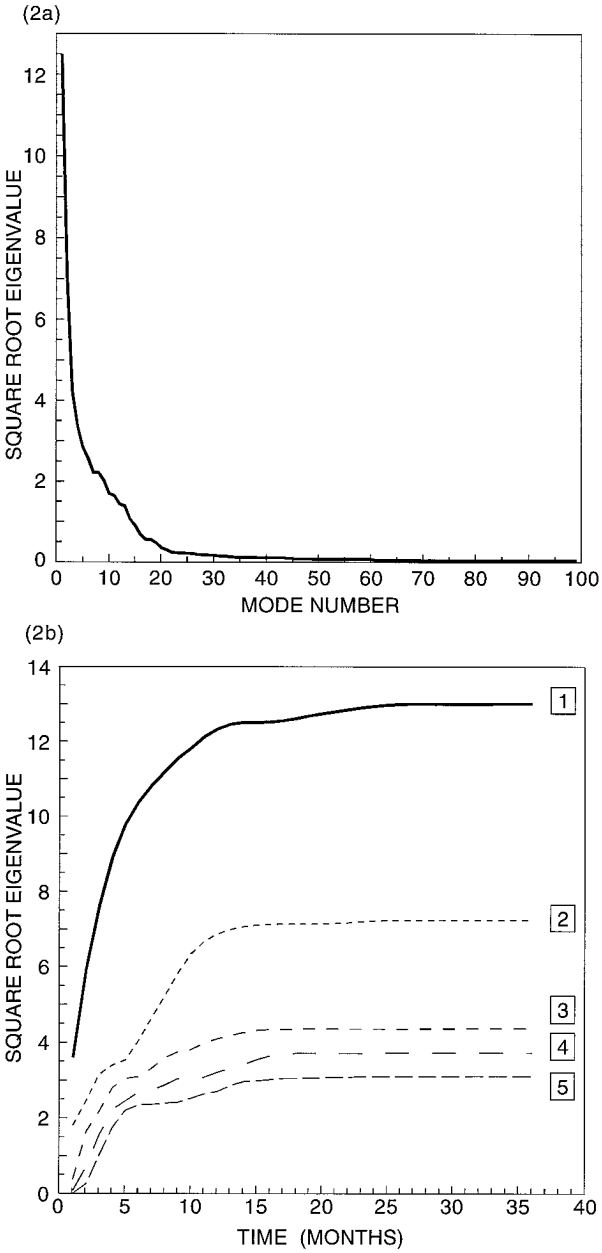

FIG. 2. (a) Square root of optimal eigenvalues at 12-month integration. (b) Variation of the square root of the first five optimal eigenvalues with integration time.

Calculating the full eigenvector/eigenvalue set for the matrix **Z** is at first sight a rather daunting task. Ostensibly one needs to integrate the adjoint model out to each time in the time sum that makes up **Z** and then apply the tangent linear model to return to the initial time of the optimal. To define **Z** as a matrix, this needs to be done to every basis vector of state space. The state vector for the coupled model has dimension 1800, and the time step of the model is around 1.5 days, which

[3] The initialization technique used by Chen et al. (1995) with the Zebiak and Cane coupled model results in skill that probably exceeds that obtained to date with the model used here.

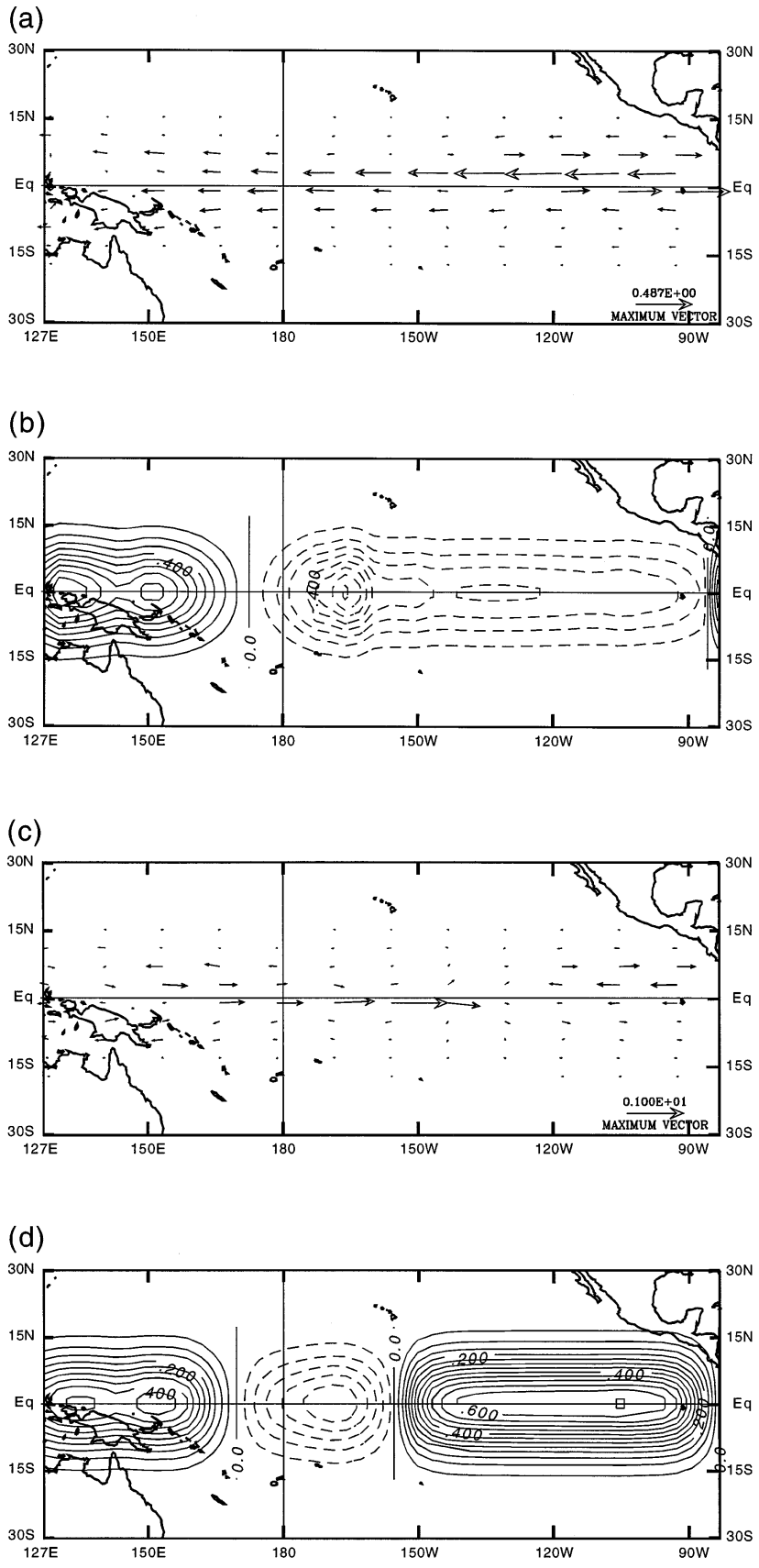

FIG. 3.

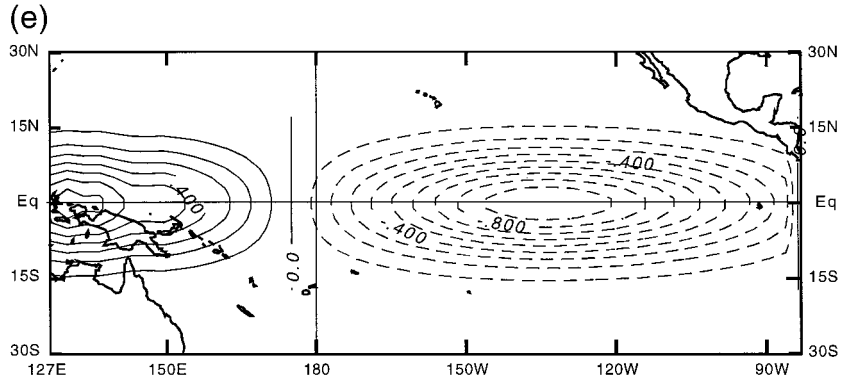

FIG. 3. (*Continued*) (a) Spatial pattern for windstress of the dominant optimal at 6-month integration. Units are dimensionless. (b) Identical to (a) but for heat flux. (c) Identical to (a) but for the second optimal. (d) Identical to (b) but for the second optimal. (e) Identical to (b) but for a simplified atmospheric model (see text).

implies that if a 6-month stochastic optimal is desired then order 10^5 integrations of an average duration of 3 months are at first sight required to evaluate $\mathbf{Z}$. Such an undertaking is close to impractical even with the current highly simplified and optimized model. Fortunately, if we restrict our attention to examining the variance of spatially averaged quantities such as NINO3 then the outlook is considerably brighter. If we denote by $\mathbf{t}_\lambda$ the vector $\mathbf{B}^\dagger(\mu, \lambda + 1)\mathbf{R}$ [cf. Eqs. (10) and (11)], then it is easy to show that

$$\mathbf{Z} = (\Delta t)^2 \sum_{\lambda=0}^{\mu-1} \sum_{\pi=0}^{\mu-1} D^{\lambda\pi}(\mathbf{t}_\lambda)(\mathbf{t}_\pi)^\dagger. \tag{15}$$

We require therefore only N backward integrations of the adjoint coupled model where $N \equiv T/\Delta t$ is the number of time steps for the time interval T of interest. In the case of the 6-month optimal discussed above, this amounts to only 120 integrations of an average duration of 3 months, that is, a 30-yr integration of the model. Given this situation, it was considered practical to calculate the stochastic optimal matrices out to 3 yr.

As the standard experiment, optimals were calculated using only the seasonal cycle as the background state (this only influences the atmospheric model) and commencing in August. Sensitivity of the results to different background states and start months are examined below. In addition, the stochastic forcing was assumed to be white in time. In actual fact (see next section), the decorrelation timescale of the observed forcing can be on the order of a few days, but this has very little qualitative effect on the dominant optimals because the coupled timescale is much longer. Hence for simplicity we confine ourselves here to white noise. The stochastic forcing was inserted as a source term in both the momentum and SST equations of the ocean. We are therefore considering a situation where both wind stress and heat flux ''noise'' are assumed to force the coupled model. Usually only momentum forcing is considered in the ENSO context, but recent field programs in the western Pacific have emphasized the importance of the latter quantity in the context of high-frequency atmospheric variability (e.g., Lukas 1987). As we shall see later, obtaining reliable estimates of the heat flux is presently difficult, so we include it only to examine in a qualitative sense what heat flux spatial signals are efficient at forcing large-scale SST signals in the coupled system. We defer consideration of the *relative* importance of wind stress and heat flux forcing to a later study when more reliable estimates of the latter quantity become available.

Depicted in Fig. 2a is the square root of eigenvalues of the first 100 optimals for 12-month integration (behavior is insensitive to integration time). Physically, each eigenvalue is proportional to the variance growth contributed by its optimal if the stochastic forcing were to project equally onto each optimal. Of course it needs to be emphasized that the magnitude of this projection depends on the degree to which the spatial coherency of the stochastic forcing matches the spatial pattern of the optimal. Notable is the sharp decline of ''instability'' or ''excitability'' with optimal number. Such a result is apparent at all integration times, as can be seen in Fig. 2b, which shows the variation of the first five eigenvalues with time. The first optimal is dominant particularly for small times and, if the noise were to project equally onto the optimals depicted, then this optimal would account for roughly four–nine times the variance growth of the next most excitable optimal.

The spatial structures of the first two optimals for 6-month integration are displayed in Fig. 3. Depicted are both the wind stress and heat flux optimal patterns. The wind stress pattern is characterized by fairly broad-scale symmetric and zonally dominated structures. This zonality is an important point since it implies that the meridional component of the wind stress noise is unimportant in causing error growth. Such a result may, of course, be model dependent given the simplicity of the current model so some caution needs to be exercised.

The dominant optimal's wind stress pattern differs

markedly in the western and eastern Pacific. In the former area, the meridional structure is reasonably broad scale, implying a better match with observed atmospheric patterns than in the east where the pattern is fairly complex. On the other hand, the signal generally appears of larger amplitude in this latter region and becomes more so as the integration time increases (the general *qualitative* response depicted in Fig. 2 is not affected much by integration time). We return to this issue in the next section when we examine observational estimates of the noise.

The heat flux shows a rather interesting pattern for the dominant optimal that is essentially independent of integration time. It consists basically of a dipole pattern confined to the western part of the basin. This result is rather surprising since the variance of NINO3 is being examined and this is an eastern Pacific SST index. Intuitively one may have expected that heat flux noise directly overlying NINO3 may have been more effective in inducing error growth. That this is not the case points to the fundamental importance of coupled dynamics in determining the response of the model to noise forcing. It is rather interesting to also note that there is some resemblance between the pattern displayed and the observations of the latent heat flux forcing of the Madden–Julian oscillation recently reported by Jones and Weare (1996; C. Jones and B. Weare 1997, manuscript submitted to *J. Climate*).

Given this western Pacific confinement, one might expect that the nature of the atmospheric model used may play some role in determining the structures observed. As was noted above, this model is spatially nonuniform (and realistically so) in its response to SST anomalies. There is a significantly larger atmospheric response in the high-mean SST western Pacific than in the low-mean SST eastern Pacific. In order to explore this, the atmospheric model heating was simplified to make it simply proportional to SST anomaly. Such an atmospheric model is purely linear in its response to SST anomalies. The resulting dominant heat flux optimal is depicted in Fig. 3e, where it is evident that the dipole pattern remains but has now spread and changed so that the eastern node of the pattern is now more dominant and overlies the NINO3 region. Thus the non-linearity of the atmosphere is an important but not total explanation for the structure observed, since the dipole pattern remains even when this characteristic is removed.

The seasonal dependence of the results are now examined by commencing the integration in February. Based on the experience of studying conventional optimals (Moore and Kleeman 1996), we might expect variance growth to be greater through the first 6 months or so of this case than the standard case. Such an analysis is confirmed by a viewing of the first eigenvalues for the dominant optimals of the two cases (Fig. 4). We see that the eigenvalues diverge between 2 and 8 months and subsequently converge over the next 6 months, consistent with the period April–September being most favorable for error growth in the model. The spatial structures of the optimal (not shown) are essentially unchanged from the standard run.

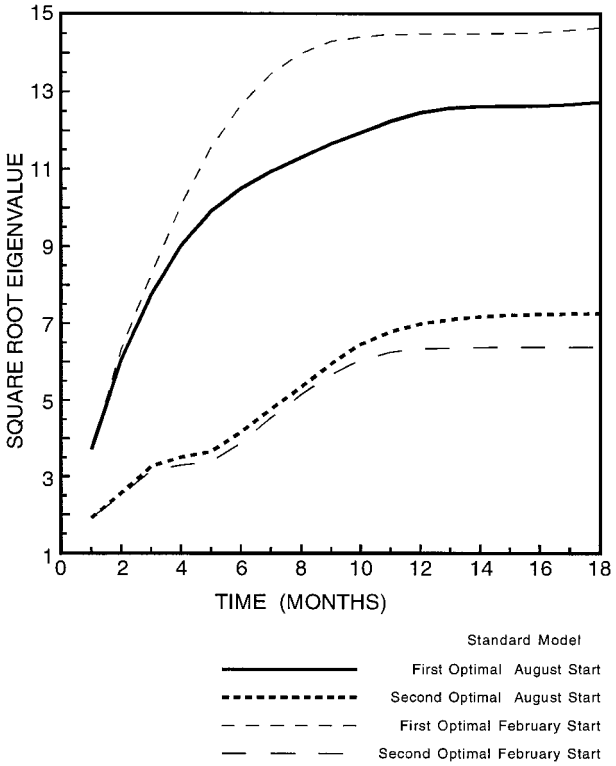

FIG. 4. Variation of the square root of the first two optimal eigenvalues with time for both an August start date (standard model) and a February start.

The model with standard parameters as described in Kleeman and Power (1994) is stable in the sense that oscillations within the model invariably decay with a timescale of a couple of years. If the coupling strength of the model is increased by around 15%, then self-sustaining oscillations with a period of about 3 yr appear. The influence of this primary bifurcation on stochastic optimals was examined by increasing the coupling strength mean wind speed parameter from 6.5 m s^{-1} to 9.0 m s^{-1}. When this was done (Fig. 5) the eigenvalue of the dominant optimal increased substantially as expected intuitively, and now significant growth also occurred at longer timescales. This was unlike the standard case where there was a saturation in growth at around 6–12 months. Interestingly, this growth occurred primarily during the April–September period of the second year, again demonstrating the significance of the seasonal cycle to variance growth. As in the seasonal cycle experiment above, the spatial structures of the dominant optimal were qualitatively unaffected by an increase in coupling strength.

Finally, we examine the influence of ENSO phase on the optimals. We do this in the same way as was previously done for the standard optimals in Moore and

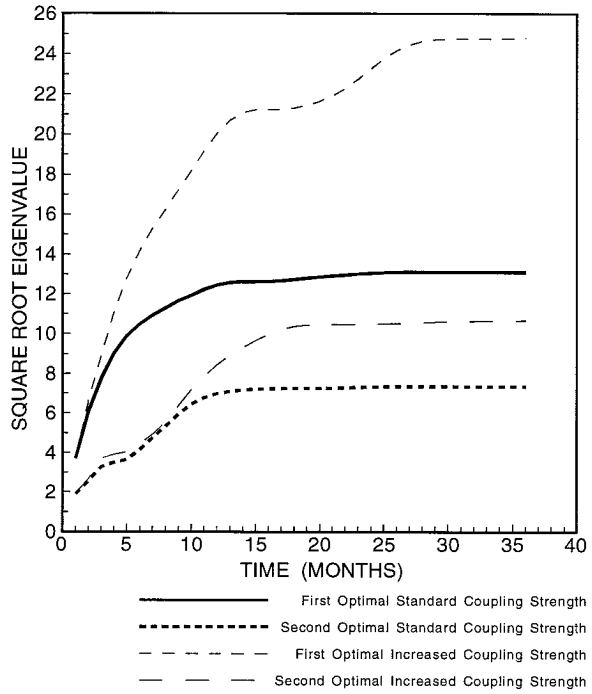

FIG. 5. Variation of the square root of the first two optimal eigenvalues with time for both the standard model and the increased coupling strength model.

Kleeman (1996): self-sustaining oscillations from the coupled model (see above) were used to define a background state for the calculation of optimals. Two starting points were used, one 6 months before a large eastern Pacific warming and the other 18 months later, which was 6 months before an analogous cooling. These starting points and the oscillation used to define the background state are depicted in Fig. 6a. Figure 6b depicts the eigenvalues of the first two optimals for both start dates, and it is clear that the dominant eigenvalue is far greater in the warm event precursor situation, as was noted in the standard optimal case. The spatial pattern of the optimals exhibits some change with phase also (not shown). The warm precursor situation resembles the standard experiment qualitatively but has a more prominent signal in the central Pacific. The cold precursor again resembles qualitatively the standard experiment but shows a significantly stronger eastern Pacific signal, probably because conditions there are very warm for much of the integration (cf. Fig. 6a). Both these results point to the importance of the SST background state. The system in both cases appears more sensitive in regions where the background SST is higher than climatology.

What are the implications of the above results for ENSO predictability? As we have seen, the eigenvalue of the first stochastic optimal tends to be larger than those of succeeding optimals. This suggests that this optimal will dominate error growth character within the coupled system. This conclusion assumes that the spatial coherency of the real world noise has sufficient similarity

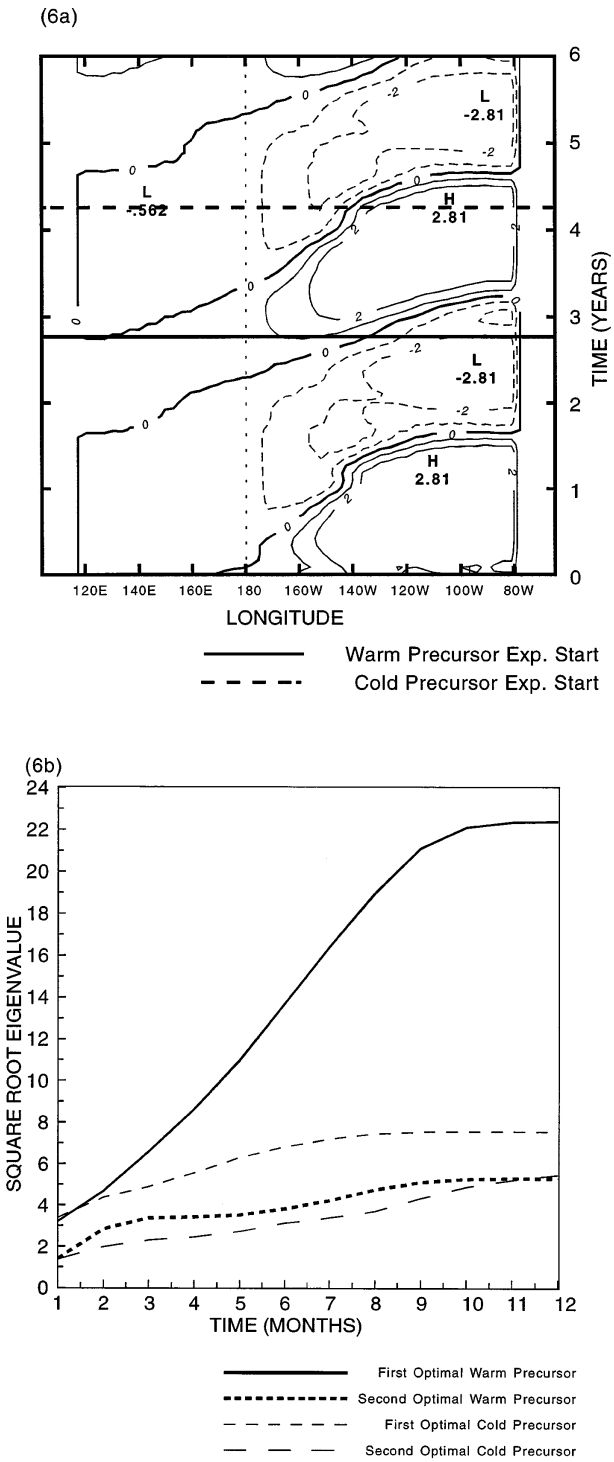

FIG. 6.(a) Hovmöller diagram of equatorial SST showing the background state used for warm and cold precursor experiments detailed in the text. (b) Variation of the square root of the first two optimal eigenvalues with time for both the warm and cold precursor experiments.

with the spatial structure of the first optimal to allow a significant projection [cf. the inner product on the right-hand side of Eq. (13)] and hence error growth. We shall see in the next section when we derive an estimate of the real world noise that this assumption is justified.

The character of the square root of the first optimal thus tells us what *kind* of error growth we may expect in the coupled system due to stochastic input. Viewing Fig. 5 we see that error growth tends to be very rapid for the first few months, after which it is substantially reduced. If the coupled system is above the primary bifurcation (i.e., capable of self-sustaining oscillations), then further reduced growth occurs on longer timescales (years), whereas if it is below the bifurcation there tends to be very little growth beyond 10 months. The *degree* to which predictability is lost depends on the ratio of the error at a given time to the standard deviation of the observed ENSO signal. Thus if the two are comparable, one would say that all predictability has been lost, whereas if the error is significantly smaller, then clearly some degree of predictability still remains. The magnitude of this ratio depends not only on the eigenvalue of the optimal but also on the size of the noise (via the eigenvalues p^j of its EOFs) and the degree to which it is able to force the optimal [via the projection in Eq. (13)]. These latter two factors are addressed in the next section.

4. Stochastic forcing

In this section we obtain an estimate of the actual stochastic component that forces the coupled system and examine how it projects onto the stochastic optimals discussed in the previous section. For our present purposes, we shall restrict our attention to the wind stress component of such forcing (see, however, the discussion section below). We do this because such a component is likely to be more reliably determined from analyses since it depends primarily on one field quantity, namely the surface vector wind. Heat flux, on the other hand, depends on a large number of field variables (air temperature, relative humidity, cloud cover, and wind speed) and so is likely to be less accurately defined in existing analyses. In order to avoid potential aliasing problems arising from monthly averaging, and also to obtain a better estimate of the spatial patterns of atmospheric transients, we opted to use the European Centre for Medium-Range Weather Forecasts (ECMWF) daily analyses (0000 UTC) for the period 1987–92 to extract the wind stress noise. Although this dataset has its problems (e.g., C. Jones and B. Weare 1997, manuscript submitted to *J. Climate*), it represents one of the best comprehensive daily datasets currently available. It is expected that better datasets will become available following the recent valuable reanalysis projects being conducted at ECMWF and National Centers for Environmental Prediction (formerly the National Meteorological Center) (see WGNE 1995) and that the present analysis could then be repeated. Following C. Jones and B. Weare (1997, manuscript submitted to *J. Climate*) we chose to correct the wind speed derived by a constant relative factor. These authors found that for the period 1985–89 a multiplicative factor of 1.4 was appropriate when comparison was made with Comprehensive Ocean–Atmosphere Data Set. We repeated their comparison on a year by year basis for the 6 yr of the dataset and found that this factor was appropriate for the first 2 yr, but that the bias was significantly reduced for the final 3 yr where a factor of 1.15 was found more appropriate. Such a result is consistent with the analysis of this dataset by Trenberth (1992), who found that the tropical circulation strengthened significantly following major revisions to the ECMWF model in May 1989. We therefore applied the first multiplicative correction factor up to this date and the second factor for the remainder of the dataset.

The extraction of the stochastic component from time series is fraught with difficulties. Many different approaches have been devised in the literature and a fairly comprehensive discussion may be found in, for example, Priestley (1981). Here we shall use two different methods and show that they give similar answers. This insensitivity of outcome adds confidence to our estimate of the noise.

The first technique used, a high-pass time filter, is probably the most obvious conceptually. Kleeman and Power (1994) found that a cutoff of periods greater than 12 months was appropriate, since it was at this point that the atmospheric model used there (and here) began to correlate significantly with observed wind when forced with observed SST. In general, the atmospheric model response compares very well with the observations for low frequencies (see Kleeman 1991; Kleeman et al. 1992). The lack of correlation at high frequencies is mainly due to the internal variability of the real atmosphere, which is what we are attempting to define here. Of course, with a more sophisticated atmospheric model (e.g., a general circulation model) there may be frequencies less than 12 months that are still a response to SST forcing. As we shall see below, however, the residual after high-pass filtering shows little autocorrelation beyond synoptic timescales, suggesting that this caveat on our method is probably not serious. Thus our first estimate of wind stress noise was obtained as follows. The 10-m winds were converted to a wind stress using a quadratic stress law and an exchange coefficient $c_D = 1.5 \times 10^{-3}$. The vector wind stress was then interpolated onto the domain used in the previous section for the stochastic optimals. The annual cycle was removed using monthly means over the 6 yr of the dataset. A high-pass filter with periods greater than 12 months removed was then applied.

The second method used involved the construction of a linear statistical model of the wind stress anomalies as a function of the observed SST anomalies (see Reynolds and Smith 1994). The noise was then derived as a residual since it is the part of the wind stress unexplained by SST variations. This linear model of the coupled

system is supported by the statistical analysis of Penland and Sardeshmukh (1995). Symbolically the model can be expressed as

$$\mathbf{w} = \mathbf{Asst} + \mathbf{n}, \tag{16}$$

where **w** is the wind stress vector defined at all spatial points of interest. Here, **sst** is the SST anomaly defined in an EOF expansion space (we used the first 10 EOFs of SST for latitudes 40°N to 40°S; results are insensitive to the addition of further EOFs). Finally, **n** is the desired signal, while **A** is the regression matrix that is obtained from the wind stress and SST datasets under the assumption that SST variations are uncorrelated with the noise **n**. A caveat on this method of noise derivation is the fact that it takes no account of the nonlinear response of the atmosphere to SST anomalies and so may conceivably overestimate the noise as a consequence.

The similarity of the resulting noise datasets was assessed by calculating the first 50 EOFs and comparing both the spatial patterns and the explained variances. It is evident from Eq. (13) that this is the appropriate comparison to make when one is interested in determining the effect of the noise on the coupled system. Rather surprisingly perhaps, there was little difference in both the spatial patterns and the explained variances of the two methods. Occasional quantitative differences could be seen after EOF number 4 but no qualitative differences were noted. In addition, eigenvalues (explained variances) were invariably within 5% of each other.

The spatial patterns of the first 5 EOFs of the high-pass dataset can be seen in Fig. 7, where it is evident that the patterns have a large-scale synoptic character. Such a synoptic interpretation is confirmed by a calculation of the autocorrelation function of the component time series of the EOFs. This shows a typical *e*-folding decorrelation timescale of around 3.5 days for the first 15 or so EOFs, dropping to around 1 day for the next 150. Higher-order EOFs show little spatial organization and an essentially instantaneous (white) decorrelation timescale. This suggests that they may be more related to analysis errors.

We now use Eq. (13) to examine the way in which the observed noise projects onto the stochastic optimals. The results to be discussed were insensitive to the particular noise dataset utilized. For our present purposes we shall assume that the noise EOFs have an exponential decorrelation character with time constants as discussed in the previous paragraph. This assumption of nonwhiteness for the low-order EOFs is important to the magnitude of the variance they excite in the coupled model but does not affect the nature of the low-order optimals to any great extent. The nonwhiteness alters the optimal operator by including cross terms with time differences of the order of the decorrelation timescale of the noise. Since this timescale is much smaller than that of the coupled model (days rather than months), the cross terms are approximately equal to the diagonal term, and so the optimal operator is modified only by a multipli-

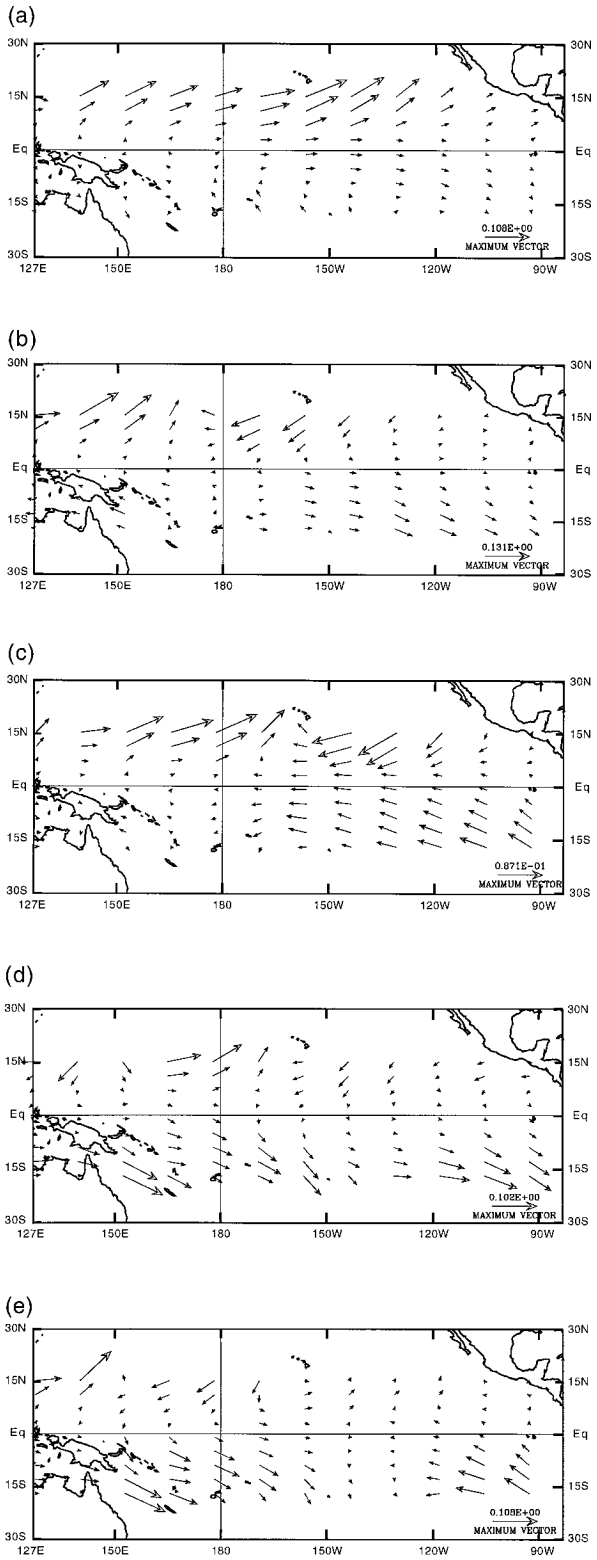

FIG. 7. The first 5 EOFs of wind stress noise derived from ECMWF analyses. The EOFs have been normalized.

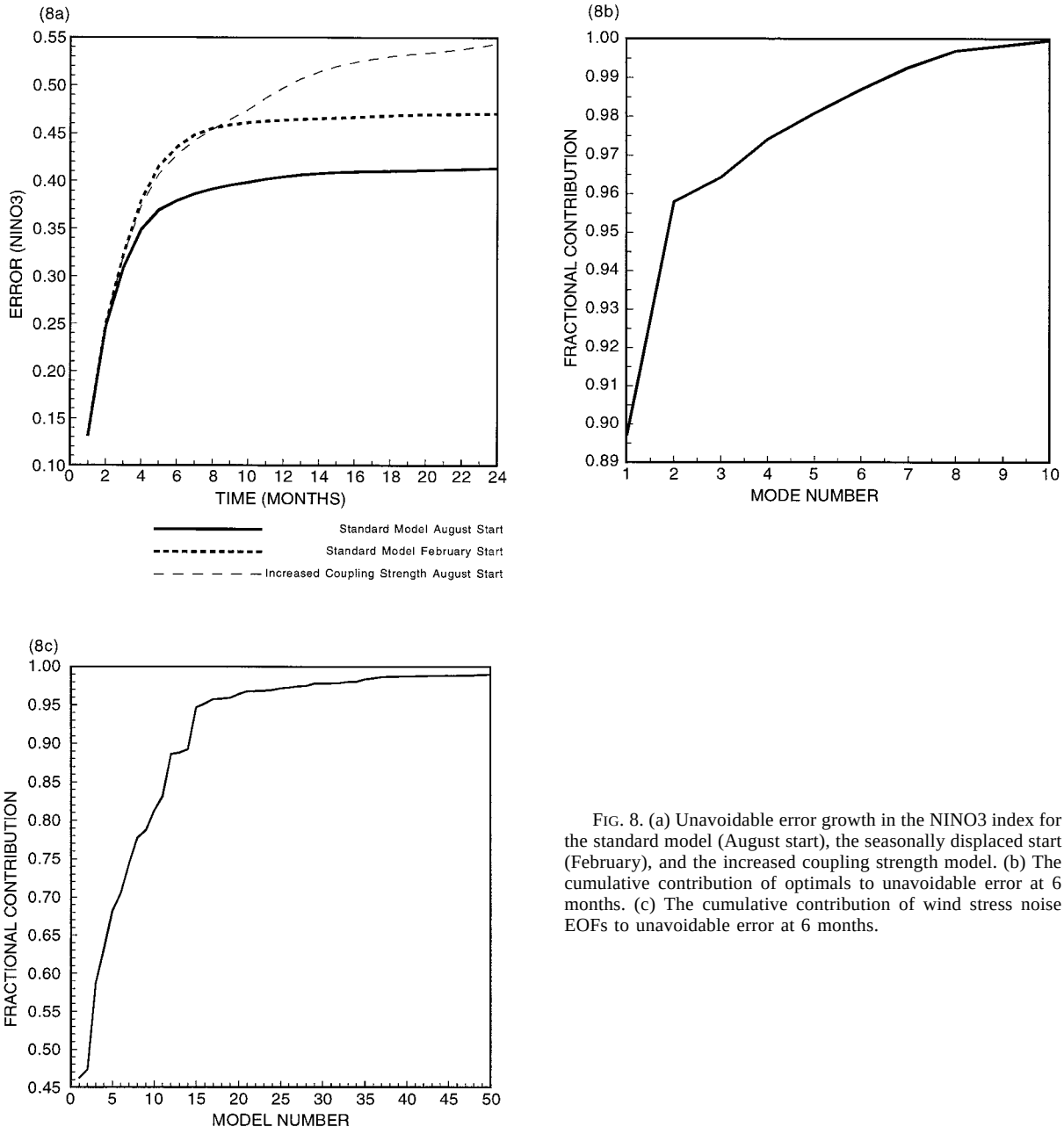

FIG. 8. (a) Unavoidable error growth in the NINO3 index for the standard model (August start), the seasonally displaced start (February), and the increased coupling strength model. (b) The cumulative contribution of optimals to unavoidable error at 6 months. (c) The cumulative contribution of wind stress noise EOFs to unavoidable error at 6 months.

cative factor. The factor is approximately equal to twice the time integral of the decorrelation function assumed. These conclusions were confirmed by calculating the nonwhite (with decorrelation timescale of 3.5 days) optimals and their eigenvalues at 6 and 12 months for the standard model discussed in the previous section. A further complication arises from the fact that several timescales are involved in the noise. This therefore violates the assumption we made in section 2 that the noise is separable in space and time. Fortunately, because we have separated the time decorrelation along EOF lines, we need only a very minor generalization of the formalism derived. In fact, since the associated time series of different EOFs are uncorrelated, it is easily shown that the components of the noise with different timescales are uncorrelated and thus expression 10 breaks into separate pieces for each of these parts of the noise.

The square root of the variance growth (the ''unavoidable''[4] error) was calculated for three cases: where

[4] The error is unavoidable because it is induced by the forcing of the climate system by atmospheric variability (primarily synoptic transients), which is essentially unpredictable beyond a few days.

forecasts were initiated in August and February and where the coupling strength was increased to induce self-sustaining model oscillations (as per the previous section). Results are displayed in Fig. 8a and show rapid growth in the first 4–6 months and a saturation at values ranging from 0.4°C to 0.55°C. They also confirm the conclusions reached on error growth in the previous section regarding seasonality and coupling strength. Surprisingly perhaps, the results are comparable with those obtained by Kleeman and Power (1994) with a quite different noise dataset (they used the monthly The Florida State University product). One difference from the results of these authors is that at quite short timescales (less than 3 months), the error growth tends to be somewhat reduced in the present case. Preliminary results from a coupled general circulation model (T. Stockdale 1996, personal communication) support this reduced short timescale error growth rate. It is interesting to contrast the error growth curve here with that obtained when initial conditions are subject to small errors. In this latter case, for standard coupling strength after an initial growth, there is a reduction because the system is essentially dissipative on asymptotically long timescales (it is below the primary bifurcation). Physically, the error saturates in the stochastic case because for long timescales the stochastic forcing balances the dissipation (see Penland and Sardeshmukh 1995; Gardner 1985).

It is instructive to decompose the error growth into its optimal and noise EOF contributions. Displayed in Figs. 8b and 8c are these decompositions for 6 months. Focusing first on the optimal decomposition (Fig. 8b), we note that error growth is overwhelmingly dominated by the contribution of the first optimal, which was analyzed in detail in the previous section. This dominance becomes somewhat less pronounced at longer integration times (the first optimal contributes around 65% of error growth at 12 months) but nevertheless it shows that the conclusions reached in the previous section regarding the sensitivity of the dominant optimal eigenvalue are likely to carry over to error growth in general (as is partially evident from Fig. 8a).

The noise EOF decomposition (Fig. 8c) is also interesting because it shows that the first 10 or so EOFs are responsible for around 90% of growth. This lends weight to our estimate of unavoidable error since it implies that most growth is induced by noise patterns that have a clear synoptic character (the first 15 or so, see above) rather than by patterns that are probably associated with analysis error (there are around 2000 patterns in all for the domain considered). These latter patterns appear to account for only around 5% of error growth.

Finally, the spatial dependency of the noise forcing was calculated. This was done to determine which spatial features of the optimals are important for exciting variance growth. The relative contribution of each grid point to variance growth is depicted in Fig. 9 for the standard model at 6 months and shows a clear central equatorial Pacific peak. This provides evidence that it is this feature of the dominant optimal rather than the meridionally complex but large eastern Pacific pattern that is primarily responsible for error growth.

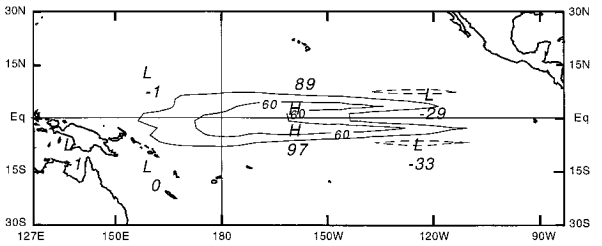

FIG. 9. The regional contribution to error growth of zonal wind stress noise. Values displayed are in °C × 10^{-7} and are for one grid point (the grid for the domain displayed is 48 zonally by 18 meridionally).

5. Summary and discussion

It has been argued that stochastic forcing of the tropical coupled ocean–atmosphere system by atmospheric transients is likely to be a major factor in the fundamental limitation of ENSO predictability. The nature of this limitation has been explored using a skillful intermediate ENSO forecast model and a newly developed theoretical framework. The major new concept in this theoretical framework is the so-called stochastic optimal, which represents the spatial patterns onto which stochastic forcing must project to maximize error growth over a given time interval. The stochastic optimal contrasts with the conventional error optimal much discussed in the literature, which shows the spatial patterns in initial conditions errors most prone to growth.

It is demonstrated that the stochastic optimal spectrum is dominated in general by the first optimal. The eigenvalue of this optimal, which measures its potential for inducing error growth, shows sensitivity to season, coupling strength, and ENSO phase. The value increases most strongly during the northern spring, increases markedly as the coupling strength increases, and tends to grow most rapidly just prior to warm events. These features have already been noted for the conventional optimals of the coupled model as analyzed by Moore and Kleeman (1996). Such a result was expected intuitively because of the mathematical relationship between the two kinds of optimals. For white noise, the stochastic optimal operator is the time integral (over the period of interest) of the conventional operator and thus represents the time average conventional optimal operator. While such a relationship is very suggestive, it should be stressed that it does not rigorously imply that the stochastic optimals are the time average of the standard optimals.

The spatial features of the dominant optimal were found to be reasonably insensitive to both the time period considered and also the parametric variations discussed above. In general, the spatial pattern for wind

stress showed large-scale characteristics both zonally and meridionally in the western to central Pacific. In the east, large amplitude features were noted, but they had a meridional scale unlikely to match observed atmospheric variability. Meridional stress was noted to be very small in the optimal, implying that the coupled model is quite insensitive to such stochastic forcing. The heat flux pattern showed a very interesting western Pacific zonal dipole that was unexpected. The error growth norm used in this study was NINO3, an eastern Pacific region, and one may have expected intuitively that heat flux noise directly overlying this region would contribute most to SST error growth here. That this is not the case points to the central importance of coupled dynamics in determining error growth.

Next, an estimate of the actual stochastic forcing of the tropical Pacific was obtained using recent ECMWF analyses. Attention was restricted to wind stress forcing as this was considered most reliable (see, however, the discussion on heat flux below). Two very different techniques were used to extract the ''stochastic'' component of the analyses, and the almost identical results obtained add to our confidence in the estimate. An EOF analysis of the stochastic dataset was performed as this was the appropriate mathematical decomposition for projection onto the optimals. The first 15 or so EOFs displayed strong synoptic character with large spatial scales and an *e*-folding decorrelation timescale of roughly 3.5 days. These patterns overwhelmingly dominated the calculated error growth, providing us with physically based confidence in our estimate of the fundamental limitation to predictability due to windstress noise. Physically, this fundamental limitation occurs because the wind stress variability associated with synoptic transients significantly forces the coupled system but, on the other hand, is essentially unpredictable beyond a week or so (as evidenced by its decorrelation timescale of 3.5 days). Thus our lack of knowledge of the synoptic state of the tropical Pacific several months in advance implies that there is a significant lack of precision in our future knowledge of slowly varying climatic quantities such as SST.

The total error growth calculated tended to grow very rapidly for the first 4 to 6 months and then saturate at a value of around 0.5°C for the NINO3 region. This behavior was reasonably similar to previous estimates obtained directly and with a very different stochastic dataset (see Kleeman and Power 1994). Confirming the previous discussion on the dominance of the first optimal, it was found that its contribution to total error growth was greater than 50% for the first 2 years. It is also worth comparing these estimates with the standard deviation of the observed NINO3, which for the period 1950–93 is around 0.82°C. Thus our estimate of error growth indicates that while a substantial amount of predictability is lost during the first 24 months due to stochastic atmospheric transients, some still remains.

The degree to which the kind of error growth calculated and analyzed here compares with growth due purely to initial condition errors (and not due to unpredictable atmospheric transients) remains a little unclear. As was noted in section 1, the degree of error growth due to the latter mechanism seems to vary according to the model used. Such variation is apparently connected to whether the model exhibits chaotic behavior or not. Despite this variation, it is still the case that the error growth reported here is much more rapid than any of the initial condition error growths reported in intermediate coupled models. This suggests strongly that on short timescales (6–12 months), the mechanism of error growth proposed here and in Kleeman and Power (1994) will dominate. On longer timescales, the issue is far from settled and seems to depend on whether the real coupled system is above or below the primary bifurcation (note the difference in behavior between 12 and 24 months in Fig. 8a according to location about the bifurcation) or whether it is in a chaotic part of parameter space. These questions await a more comprehensive study that is currently being planned.

Some preliminary discussion of the contribution of heat flux stochastic forcing is warranted. Clearly an analysis similar to that performed above for wind stress is required; however, reliable observational estimates of heat flux are only now just beginning to appear. Two studies of particular interest in this regard are those of Jones and Weare (1996; C. Jones and B. Weare 1997, manuscript submitted to *J. Climate*) and Hendon and Glick (1997). Both have concentrated on the heat flux signature of the Madden–Julian oscillation and reached a number of conclusions relevant to the work here. The first authors restricted their attention to the evaporative component of the flux and showed that, in the eastward propagating oscillation, reduced upward flux tended to lead the equatorial westerly wind anomalies and convection, while increased upward flux tended to lag. Such a pattern corresponds quite well with the dominant optimal calculated here (cf. Figs. 2a,b). Hendon and Glick also considered the radiative component of the flux and argued that it was generally greater than the evaporative component. This radiative component was essentially due to cloudiness changes that are generally coincident with the westerly wind anomalies. Thus the latent heat component of the flux is likely to add to error growth, while the radiative component appears likely to be neutral. Of course, it should be stressed that these conclusions are tentative, and a more comprehensive study is currently being planned.

Finally, it is worth emphasizing that the results derived here were made using a relatively simple coupled model (an ''intermediate'' model). For this reason some caution needs to be exercised in interpreting the results, as they may be model dependent. Clearly our results will need to be carefully compared with those obtained with other skillful ENSO forecast models. Despite this reservation, we feel that the results discussed here have considerable credibility because the model from which they have been obtained is particularly skillful at ENSO

forecasting (see Kleeman et al. 1995) and is able to produce an ENSO oscillation that is reasonably realistic in both its zonal structure and its evolution (see Kleeman and Power 1994).

APPENDIX

Positivity of the Stochastic Optimal Operator

We demonstrate here that the eigenvalues of the stochastic optimal operator **Z** and the noise covariance operator **C** are all nonnegative. Equivalently, we demonstrate that these two operators are *positive* (Lipschutz 1974). First we note because of the definition of a norm that **X** the norm kernel matrix is positive.

In the case of **C**, it is obvious that it is positive since, in a basis in which this noise covariance matrix is diagonal, the diagonal elements are simply the variances of the transformed noise fields (i.e., a linear combination of the noise field at different spatial points), which are evidently nonnegative. In the case of **Z**, we note that because **X** is positive it may be written in the form $\mathbf{Y}\dagger\mathbf{Y}$ (see Lipschutz 1974). In addition, the time covariance matrix D is symmetric and all eigenvectors are nonnegative by the same argument given above for **C** being positive and is hence also positive. This implies that we can write

$$D^{\mu\nu} = E^{\mu\lambda}E^{\nu\lambda}$$

and hence

$$\mathbf{Z} = \left[\sum_{\lambda=0}^{\mu-1} E^{\lambda\kappa}\mathbf{B}(\mu, \lambda + 1)\mathbf{Y}\right]^{\dagger}\left[\sum_{\pi=0}^{\mu-1} E^{\pi\kappa}\mathbf{B}(\mu, \pi + 1)\mathbf{Y}\right],$$

which implies that it is the sum of a series of symmetric matrices of the form $\mathbf{H}\dagger\mathbf{H}$ (note the summation over κ). A simple application of the theorem on p. 288 of Lipschutz (1974) [this states that if an operator **T** is self-adjoint and satisfies $(\mathbf{T}\phi, \phi) \geq 0$ *for all vectors* ϕ then it is positive] leads to the conclusion that **Z** itself is positive.

REFERENCES

Balmaseda, M. A., D. L. T. Anderson, and M. K. Davey, 1994: ENSO prediction using a dynamical ocean model coupled to statistical atmospheres. *Tellus,* **46A,** 497–511.

Battisti, D. S., 1988: Dynamics and thermodynamics of a warming event in a coupled tropical atmosphere–ocean model. *J. Atmos. Sci.,* **45,** 2889–2929.

Blumenthal, M. B., 1991: Predictability of a coupled ocean–atmosphere model. *J. Climate,* **4,** 766–784.

Chen, D., S. E. Zebiak, A. J. Busalacchi, and M. A. Cane, 1995: An improved procedure for El Niño forecasting. *Science,* **269,** 1699–1702.

Egger, J., and H. D. Schilling, 1984: Predictability of atmospheric low-frequency motions. *Predictability of Fluid Motions,* G. Holloway and B. J. West, Eds., American Institute of Physics, 149–157.

Farrell, B. F., 1990: Small error dynamics and predictability of flows. *J. Atmos. Sci.,* **47,** 2409–2416.

——, and P. J. Ioannou, 1993a: Stochastic forcing of the linearized Navier–Stokes equations. *Phys. Fluids,* **5,** 2600–2609.

——, and ——, 1993b: Stochastic dynamics of baroclinic waves. *J. Atmos. Sci.,* **50,** 4044–4057.

——, and ——, 1993c. Stochastic forcing of perturbation variance in unbounded shear and deformation flows. *J. Atmos. Sci.,* **50,** 200–211.

Frederiksen, J. S., 1982: A unified three-dimensional instability theory of the onset of blocking and cyclogenesis. *J. Atmos. Sci.,* **39,** 969–982.

Gardiner, C. W., 1985: *Handbook of Stochastic Methods.* Springer–Verlag, 442 pp.

Goswami, B. N., and J. Shukla, 1991: Predictability of a coupled ocean–atmosphere model. *J. Climate,* **4,** 3–22.

Hadley, G., 1961: *Linear Algebra.* Addison–Wesley, 290 pp.

Hendon, H. H., and J. Glick, 1997: Intraseasonal air–sea interaction in the tropical Indian and Pacific Oceans. *J. Climate,* in press.

Jin, F.-F., J. D. Neelin, and M. Ghil, 1994: El Niño on the devil's staircase: Annual subharmonic steps to chaos. *Science,* **264,** 70–72.

Jones, C., and B. C. Weare, 1996: The role of low-level moisture convergence and ocean latent heat fluxes in the Madden and Julian oscillation: An observational analysis using ISCCP data and ECMWF analysis. *J. Climate,* **9,** 3086–3104.

Kleeman, R., 1991: A simple model of the atmospheric response to ENSO SST anomalies. *J. Atmos. Sci.,* **48,** 3–18.

——, 1993: On the dependence of hindcast skill in a coupled ocean–atmosphere model on ocean thermodynamics. *J. Climate,* **6,** 2012–2033.

——, 1994: Forecasts of tropical Pacific SST using a low order coupled ocean–atmosphere dynamical model. *NOAA Exper. Long-Lead Forecast Bull.* **3,** 10–11.

——, and S. B. Power, 1994: Limits to predictability in a coupled ocean–atmosphere model due to atmospheric noise. *Tellus,* **46A,** 529–540.

——, J. S. Frederiksen, and R. C. Bell, 1988: Statistical dynamics of quasigeostrophic flows. *Computational Techniques and Applications: CTAC-87,* Noye and Fletcher, Eds., North Holland, 685 pp.

——, M. Latif, and M. Flügel, 1992: A hybrid coupled tropical atmosphere ocean model: Sensitivities and hindcast skill. Max-Planck Institut fur Meteorologie Rep. 76, 37 pp. [Available from Max-Planck-Institut für Meteorologie, Bundesstrasse 55, D-20146 Hamburg, Germany.]

——, A. M. Moore, and N. R. Smith, 1995: Assimilation of sub-surface thermal data into an intermediate tropical coupled ocean–atmosphere model. *Mon. Wea. Rev.,* **123,** 3103–3113.

Lipschutz, S., 1974: *Theory and Problems of Linear Algebra.* McGraw Hill, 334 pp.

Lukas, R., 1987: On the role of western Pacific air–sea interaction in the El Niño/Southern Oscillation phenomenon. *Proc. U.S. TOGA Western Pacific Air–Sea Interaction Workshop,* Honolulu, HI, UCAR, 16–18.

Molteni, F., and T. N. Palmer, 1993: Predictability and finite-time instability of the northern winter circulation. *Quart. J. Roy. Meteor. Soc.,* **119,** 269–298.

Moore, A. M., and R. Kleeman, 1996: The dynamics of error growth and predictability in a coupled model of ENSO. *Quart. J. Roy. Meteor. Soc.,* **122,** 1405–1446.

Penland, C., and P. D. Sardeshmukh, 1995: The optimal growth of tropical sea surface temperature anomalies. *J. Climate,* **8,** 1999–2024.

Priestley, M. B., 1981: *Spectral Analysis and Time Series.* Academic, 890 pp.

Reynolds, R. W., and T. M. Smith, 1994: Improved global sea surface temperature analysis using optimum interpolation. *J. Climate,* **7,** 929–948.

Trenberth, K. E., 1992: Global analyses from ECMWF and atlas of 100 to 10mb circulation statistics. NCAR Tech. Note 373, 191 pp.

WGNE, 1995: Report of the tenth session. WMO/TD-No. 670, 43 pp.

Zebiak, S. E., and M. A. Cane, 1987: A model El Niño–Southern Oscillation. *Mon. Wea. Rev.,* **115,** 2262–2278.

——, and ——, 1991: Natural climate variability in a coupled model. *Greenhouse Gas Induced Climatic Change: Critical Simulations and Observations,* M. E. Schlesinger, Ed., Elsevier, 457–470.